# Multiscale Simulations of Proton Coupled Electron Transfer in Biomimetic Peptides – Supplementary Information

Katharina Spies, Leonie Pfeffer, Tomáš Kubař and Natacha Gillet

July 2, 2025

## A Classical MD – Structural Analysis

### A.1 Structures of the biomimetic peptides

The structure of the β-hairpin peptides is shown in Figures 1a and 4a–4c. Water molecules at 5 Å distance from the transferred hydrogen atom are shown to provide a view of the solvent exposure of the residues involved in the PCET reaction.

In wild-type peptide β-H14 (WT) (Figure 1a), the proton can transfer between Y5 and H14 either directly or via a water chain[1]. In peptide β-W14 (Figure 4a), the residue H14 is replaced by tryptophan (W), as tyrosine/tryptophan dyads are conserved structural motifs in various proteins[2,3]. Examples are found in the β2 subunit of RNR, with a tyrosine and a tryptophan in a staggered T-shaped arrangement[4], in PSII[5], as well as in oxidoreductases[6], cryptochromes[7] and photolyases[8]. Finally, peptide β-Y14 has H14 mutated to tyrosine in order to induce a symmetrical PCET reaction between the opposite β-strands. The V7Y mutation in peptide β-Y7 (Figure 4b) is supposed to permit a PCET mechanism between two tyrosine residues on the same strand of the β-sheet. The insets in Figure 4c show two different orientations of the tyrosines in the β-hairpin peptide β-Y14: a π-stacked (β-Y14s) and a flipped (β-Y14f) conformation. These geometries respectively correspond to the orientations of αY730/αY731 and αY731/βY356 found in RNR[9].

The secondary structure of the α-helical protein A (WT) features three α-helices, as determined by CD and NMR spectroscopy[10]. There is only one tyrosine residue in the center of the WT sequence (Y34, Figure 1b), which was thought to be buried in the protein structure[11,12]. By contrast, the protein structure changes during our simulations, exposing Y34 to the solvent, and the same event occurrs in the α-Y31 (K31Y) variant (Figure 4e). The tyrosines in the α-Y56 (V56Y) and α-Y30 (L30Y) variants (Figures 4d and 4f), however, remain buried within the three α-helices structure.

Classical MD simulations were performed to produce suitable initial structures for the QM/MM simulations, in which the residues involved in the PCET are close enough for the reaction to take place. The distances between the proton donor and acceptor atoms (nitrogen in histidine and tryptophan, oxygen in tyrosine) were measured. Structures in which this distance corresponded to a direct contact (≈ 3 Å) were used as initial structures for subsequent QM/MM simulations. A detailed analysis of the stability of the secondary structures in the classical MD simulations can be found in the next section.

### A.2 Stability of the secondary structure

Unbiased classical MD simulations were performed for 200 ns for all systems and the Root-Mean-Square Deviation (RMSD) and Define Secondary Structure of Proteins (DSSP) analyses were performed to verify that the secondary structure was conserved.

The procedure for the classical MD simulations is described in the main text in section 2.2.2. In addition, Replica Exchange with Solute Tempering (REST2) simulations were performed as in Ref. 3. The input parameters are the same as in the classical NPT equilibration and production runs. A total of 8 replicas were used and all atoms of the peptide were considered as the hot region and the lambda values were decreased from 1.00 to 0.65. The total time of the REST2 simulations was 100 ns. All subsequent analyses were performed using the trajectory of the first replica.

In all β-hairpin peptides as well as the α-helical protein mutants Y56, Y30 and Y31, one tyrosines was replaced by a radical tyrosine and an additional production run is performed with the parameters as the MD production run.

The DSSP and RMSD analysis was performed on all peptides regardless of the oxidation state of the tyrosines using VMD[13,14] and cpptraj[15]. All plots were generated using gnuplot[16] or Python[17] with the Matplotlib[18], NumPy[19], Pandas[20], and Seaborn[21] libraries.

Figure A.1 shows the RMSD with respect to the average structure of all β-hairpin peptides (Figure A.1a) and α-helical proteins (Figure A.1b). The RMSD of the β-hairpin peptides is slightly higher than that of the α-helical proteins due to the direct solvent exposure leading to an increased mobility. However, it is still less than 5 Å in all systems, emphasizing the conservation of the secondary structural motifs.

All β-hairpin peptides have a bend in the middle of the structure between residues 9 and 11 and extended β-sheets from residues 3 to 7 and 12 to 17, as shown for all β-hairpin peptides in the DSSP plots in Figure A.2. These structures are consistent with the expectations of Ref. 5. Figure A.3a shows the DSSP plots of all the α-helical proteins, illustrating the three-helical α-helical secondary structure determined by CD and NMR spectroscopy.[10] The structure is stable along the 200 ns simulation. The REST2 simulations that were performed to access a larger conformational space also show the conservation of secondary structures of all peptides.

Classical MD simulations with one tyrosine simulated as radical tyrosine were performed and similar to the results above, the overall secondary structure was conserved (see Figure A.4 and A.5). Hwang et al. describe an unfolding of β-hairpin A when the tyrosine residue is oxidized in their MD simulation.[22] This is not the case in our simulations as shown in Figure A.4a.

## B Benchmark Charges

We were also interested in the performance of the QM method that we used, so we performed a small benchmark to compare the DFTB3 results with spin polarization to DFTB3 without spin polarization, to long range corrected DFTB2 (LC-DFTB2), and to two

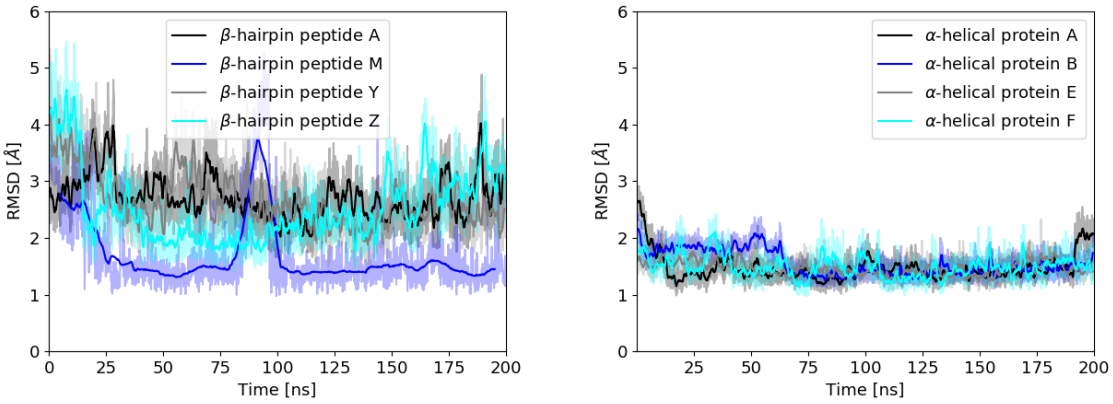


**(a)** H14 (WT), W14, Y7 and Y14 **(b)** A (WT), Y56, Y30 and Y31

Figure A.1 Secondary structure is conserved in all biomimetic peptides. RMSD Plots of (a) β-hairpin peptides and (b) α-helical proteins with respect to the average structure.

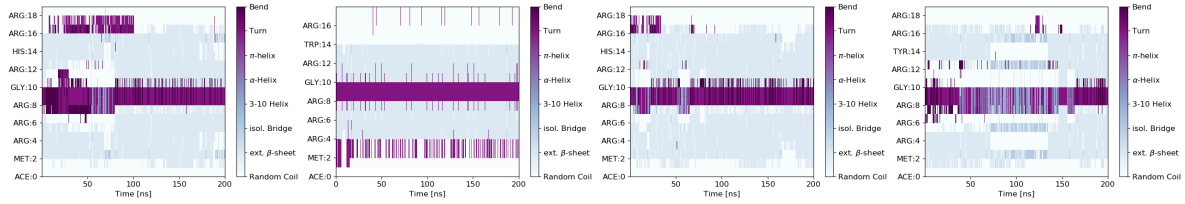


**(a)** β-hairpin H14 **(b)** β-hairpin W14 **(c)** β-hairpin Y7 **(d)** β-hairpin Y14

Figure A.2 DSSP Plots of β-hairpin peptides: Extended β-structure is stable.

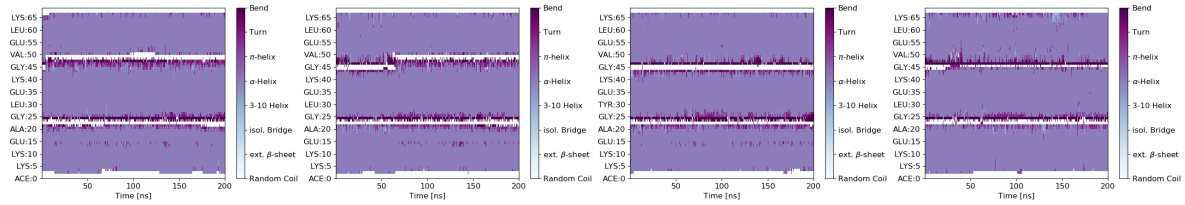


**(a)** α-helical protein A **(b)** α-helical protein Y56 **(c)** α-helical protein Y30 **(d)** α-helical protein Y31

Figure A.3 DSSP Plots of α-helical proteins: α-helical structure is stable.

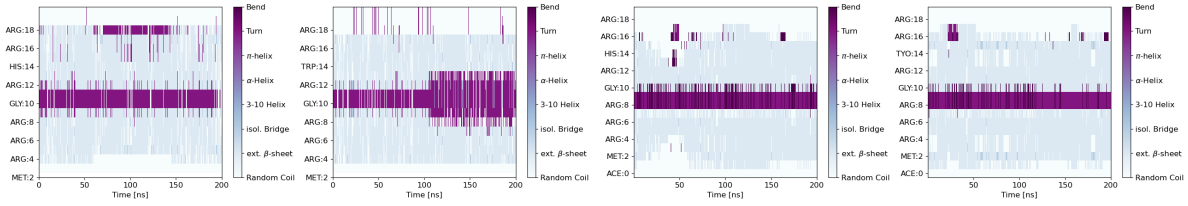


**(a)** β-hairpin H14 **(b)** β-hairpin W14 **(c)** β-hairpin Y7 **(d)** β-hairpin Y14

Figure A.4 DSSP Plots of β-hairpin peptides H14, W14, Y6 and Y14 with one radical tyrosine: Extended β-structure is stable.

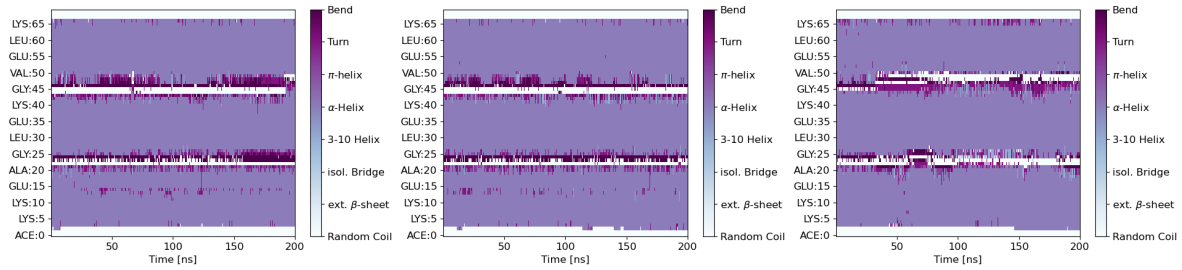


**(a)** α-helical peptide Y56 **(b)** α-helical peptide Y31 **(c)** α-helical peptide Y30

Figure A.5 DSSP Plots of α-helical proteins Y56, Y30 and Y31 with one radical tyrosine: α-helical structure is stable.

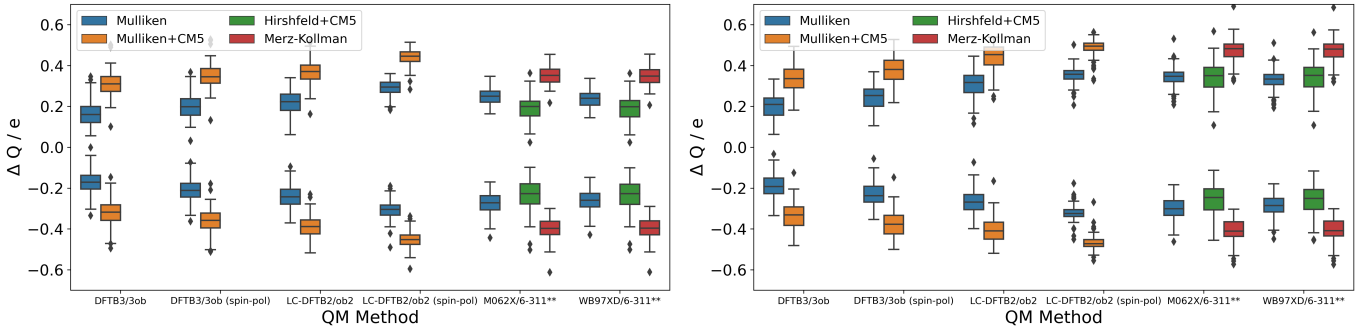


**(a)** β-Y14s **(b)** β-Y14f

Figure B.1 Benchmark of charge analysis using various QM methods and partial charge schemes: DFTB3/3OB and LC-DFTB2/ob2 (each with and without spin polarisation), as well as the DFT-methods M06-2X/6-311** and ωB97X-D/6-311**. For the DFTB methods, Mulliken charges and their CM5-corrected counterparts are used. For the DFT methods, both Mulliken and CM5-corrected Hirshfeld charges are evaluated, along with Merz-Kollman partial charges.

DFT methods: M06-2X and ωB97X-D, both with the basis set 6-311**. For systems β-Y14s and β-Y14f, 200 trajectory snapshots per system were randomly selected from the free QM/MM simulations and the coordinates of the QM atoms were used as input for the QM calculations in vacuo. . We calculated $\Delta Q$ with partial charges derived from various methods: DFT and DFTB-derived Mulliken charges, DFTB Mulliken charges with CM5 correction, DFT Hirshfeld charges with CM5 correction, and DFT Merz-Kollman charges. Figure B.1 compares the different methods.

DFTB3 without spin polarization delocalizes the charges the most, as we can see in both systems. We see that in the π-stacked β-hairpin structure, $\Delta Q$ is smaller in magnitude, not only when using DFTB3. This is due to the delocalization of the electron between the tyrosine rings. In the other system, there is no permanent π-stacking, therefore the electron is localized on either one of the tyrosine residues. Here, LC-DFTB2 and the reference DFT methods accurately describe this, while DFTB3 fails to capture the electron localization. $\Delta Q$ values are very similar across different DFT methods when compared directly. When derived from Mulliken charges, they show good agreement with values obtained from LC-DFTB methods, both spin-polarized and non-spin-polarized. In contrast, $\Delta Q$ values derived from CM5-corrected Hirshfeld charges differ significantly from those based on Merz-Kollman charges across both DFT methods. As a result, we cannot conclude that applying the CM5 correction to DFTB Mulliken charges improves the collective variable. Therefore, we employ LC-DFTB2 with spin-polarization for recalculating the electron transfer CV, as it offers a reasonable and consistent compromise.

# C Partial Charges

The electron transfer CV $\Delta Q$ is based on the sum of the partial charges of the molecules involved in the PCET reaction. For a better understanding of the 2D FES, a more detailed analysis of the charge distribution is shown in Figure C.1. The summed partial charges of the Tyr˙ molecule $Q_{\mathrm{Y}\bullet}$ are shown in red, and the summed partial charges of the PCET partner $Q_{\mathrm{H}}/Q_{\mathrm{W}}/Q_{\mathrm{Y}}$ (His, Trp or Tyr, respectively) without the proton to be transferred in blue, as well as the partial charge of the transferred proton $q_{\mathrm{H}}$ in black, and the CV for the electron transfer $\Delta Q = Q_{\mathrm{X}} - Q_{\mathrm{Y}\bullet}$ in orange.

## C.1 Unbiased MD simulations

Along the unbiased simulation of PCET between H14 and Y$^{\bullet}$ (Figure C.1a), no transfer reaction is observed, the total charge of the QM system is +1 due to the double protonated histidine. The partial charge $q_{\mathrm{H}}$ is 0.3 e, the charge of the tyrosine in radical state $Q_{\mathrm{Y}\bullet} \approx 0$ e, resulting in $\Delta Q = 0.7$ e. This results in a narrow minimum in the 2D free energy surface, see Figure 5a.

Except for the systems with histidine, all other QM regions are neutral. In the system with W14 and $Y^{\bullet}$ (Figure C.1b) the partial charge $q_H$ is 0.25 e, $Q_{Y\bullet}$ is $\approx -0.15$ e and $Q_W$ is about $-0.1$ e. Due to fluctuations in both, $Q_{Y\bullet}$ and $Q_W$, ΔQ ranges from $-0.2$ to 0.25 e. No proton transfer was observed here and in the 2D FES the minimum is stretched along the y-axis (see main text Figure 5b).

In Y14f (Figure C.1c), the partial charge $q_H$ of the hydrogen is 0.4 e, the partial charges of the two tyrosines exchange their values, depending on the proton position. The one in radical state fluctuates from 0 to $-0.3$ e, while the other one is slightly more negative, fluctuating from -0.1 to $-0.5$ e. This results in ΔQ fluctuating between -0.4 and 0.4 e and in two stretched minima at $-0.3$ and 0.3 e in the 2D FES (see main text Figure 5e).

### C.2 Metadynamics MD simulations (Proton Transfer biased)

The case in H14 is quite different in the metadynamics simulation (Figure C.1d). At the beginning of the simulation the charge distribution is similar to in the unbiased case but the partial charges of $Q_{Y\bullet}$ increase to 0.3 e when $Q_H$ decreases to the same value. $\Delta Q$ fluctuates between 0 and 0.7 e until the proton transfer occurs, then the mean value of $Q_H$ drops to 0.4 e and $Q_{Y\bullet}$ increases to 0.2 e. The charge of the transferred hydrogen $q_H$ increases slightly and $\Delta Q$ fluctuates around 0.3 e. Both minima, the narrow one at 0.7 e and the stretched around 0.3 e are observed in main text Figure 6a.

In W14 (Figure C.1e) the proton transfer leads to a change of $q_H$, which increases from 0.25 to 0.35 e. The partial charges of $Q_W$ fluctuate between $-0.1$ and $-0.3$ e, when the tyrosine is in the radical state, whereas they fluctuate between 0 and $-0.1$ e, when tryptophan is in the radical state. Regarding the tyrosine, the partial charges $Q_{Y\bullet}$ also fluctuate between 0 and $-0.1$ e, but drop to $-0.25$ and $-0.35$ e, as soon as the proton is transferred. This results in $\Delta Q$ fluctuating between $-0.15$ and 0.15 e, when the tyrosine is in radical state and it increases to 0.2 to 0.3 e when tryptophan is in the radical state. The stretched minima along the *y*-axis in the reactant state and the narrow one around 0.3 e in the product state are clearly visible in main text Figure 6b.

The comparison between the unbiased simulation of Y14 and the metadynamics simulation (Figure C.1f) shows only two small differences: the exchange rate is strongly increased in the latter, while the mean values of $Q_{Y\bullet}$ and $Q_Y$ are slightly more localized at 0 and $-0.3$ e, which results in $\Delta Q = -0.3$ or 0.3 e depending on the proton position. That is due to the recalculation of the Mulliken charges with LC-DFTB. Therefore, the minima in main text Figure 6e are localized at the mean value of $-0.3$ and 0.3 e.

## D Environmental and Structural Analysis

### D.1 Interactions between aromatic rings

We performed an analysis of the percentage of π-stacking interaction between the aromatic rings involved in the PCET reaction. We took the relationship between the centroid distance and the angles between the planes into consideration. Thresholds and conditions were adapted from Salentin et al.[23] Table D.1 shows the percentage of π-stacked interactions along the trajectory for the biomimetic peptides in the unbiased MD simulations and in the PT metadynamics simulations.

Figure D.1 shows the distances between the centers of mass (COM) of the aromatic side chains of the residues involved in the PCET reaction. Only systems with two tyrosines are shown.

### D.2 Environment of residues involved in the PCET

To analyze the environment of the residues involved in the PCET, we performed an extended hydrogen bonding and distance analysis. The analysis was performed using the hbond utility in vmd and selecting nearby residues in a 3 Å cutoff. We distinguished between water molecules and explicit amino acids in our analysis (see Figure D.2). As expected, we observe a much higher number of water molecules in the β-hairpin peptides and the α-helical protein Y31 than in the other two α-helical proteins Y56 and Y30, the latter being embedded in the protein structure. All α-helical proteins have more interactions with nearby amino acids than the β-hairpin peptides. Usually, the interacting amino acids are direct neighbors in the amino acid chain. Stacked β-hairpin Y14s and β-hairpin H14 have only a small number of other amino acids in close proximity. Table D.2 shows the averaged number of hydrogen bonds for all systems.

## E 1D Metadynamics – FES

### E.1 FES with error bars

Block averaging combined with Bayesian bootstrapping was performed on the PT metadynamics simulations to monitor the convergence and to obtain an error analysis. Figure E.1 shows that the average error becomes constant with increasing block size, which is a sign for convergence of the metadynamics simulations. A block size of 7000 was chosen to obtain the error estimate in the FES.

#### E.1.1 1D-FES Proton Transfer

The results from the 1D metadynamics simulations, in which the proton transfer reaction barrier was biased, give free energy surfaces for the proton transfer reaction coordinate (Figure E.2). The values for the PT barrier heights and driving forces in Table 2 in the main text are based on these representations. The proton transfer barrier is higher for biomimetic peptides in which the tyrosine radical and either histidine or tryptophan are involved in the PCET reaction, whereas two tyrosines lead to lower barriers. The product and reactant wells are of similar depth for β-hairpin Y7 and Y14, whereas the product state is less populated for β-hairpin peptide H14 and W14. For α-helical proteins, the well depths are similar deep, except for Y31, which favors the product state.

#### E.1.2 2D-FES with Error Estimation

Figure E.3 shows the FES of all systems, which are identical to Figure 6 in the main text as well as the corresponding error estimates. Except for β-hairpin H14 the error in the reactant and product basins is quite small. Only in β-hairpin H14 and W14 the transition state seems to have a higher error estimate than the rest of the surface.

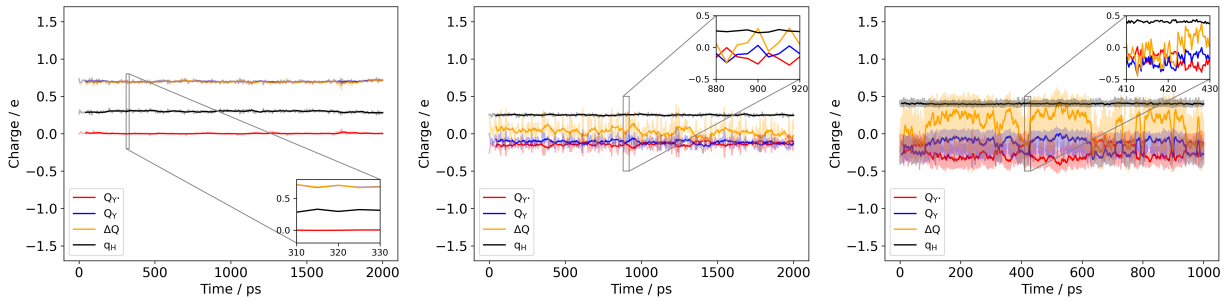


**(a)** H14 - unbiased MD **(b)** W14 - unbiased MD **(c)** Y14f - unbiased MD

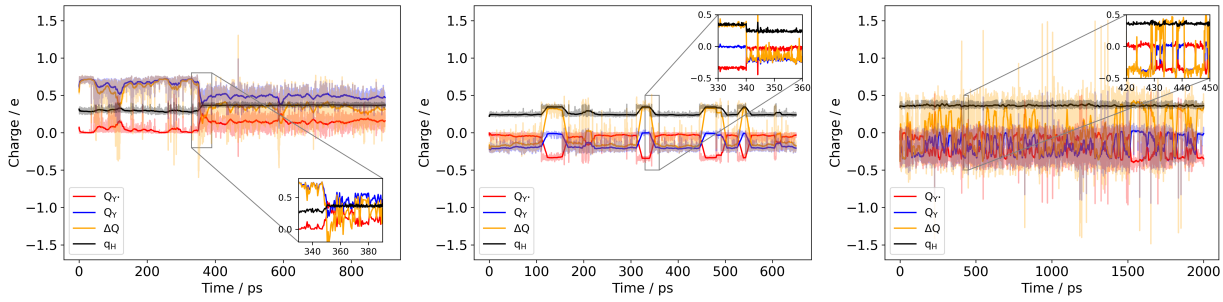


**(d)** H14 - WT-Metad **(e)** W14 - WT-Metad **(f)** Y14f - WT-Metad

Figure C.1 Partial Charges of H14, W14 and Y14f exemplarily to clarify the charge distribution on the molecules. Upper panels (a)–(c): unbiased MD simulations. Lower panels (d)–(f): selected walkers of the metadynamics simulations, in which the proton transfer was biased. Walkers were chosen accordingly that at least one transfer reaction was clearly visible.

Table D.1 Interactions between aromatic residues involved in the PCET. Relative occurrence of $\pi$-stacking. .

| | | β-H14 | β-W14 | β-Y7 | β-Y14s | β-Y14f | α-Y56 | α-Y31 | α-Y30 |
|---|---|---|---|---|---|---|---|---|---|
| free MD | π-stacked (%) | 2.49 | 69.20 | 12.02 | 80.88 | 13.38 | 4.19 | 14.58 | 0.00 |
| PT-Metad | π-stacked (%) | 5.85 | 52.74 | 12.48 | 72.10 | 24.08 | 0.00 | 7.35 | 0.82 |

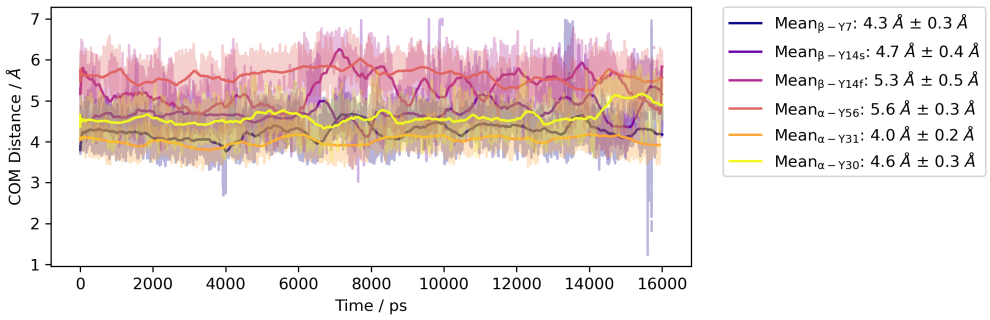


Figure D.1 Distance between center of mass (COM) of aromatic side chains of residues involved in PCET.

Table D.2 Average number of hydrogen bonds of atoms involved in the PCET reaction either to water molecules (solvent), to other amino acids residues (protein), or between the partners in the PCET reaction (Tyr˙-X, with X is His in β-H14, Trp in β-W14, and Tyr in all other systems). Criteria to be met for hydrogen bonding: (i) $\text{angle}_{\text{H-Donor}\cdots\text{Acceptor}} \leq 30^\circ$ and (ii) $\text{distance}_{\text{Donor}\cdots\text{Acceptor}} \leq 3.5$ Å.

| | β-H14 | β-W14 | β-Y7 | β-Y14s | β-Y14f | α-Y56 | α-Y31 | α-Y30 |
|---|---|---|---|---|---|---|---|---|
| Solvent | 0.97 | 0.52 | 1.43 | 1.97 | 1.67 | 0.16 | 1.59 | 0.56 |
| Protein | 0.82 | 0.00 | 0.30 | 0.06 | 0.20 | 0.25 | 0.07 | 0.08 |
| Tyr˙-X | 0.25 | 0.02 | 0.41 | 0.36 | 0.47 | 0.87 | 0.28 | 0.63 |
| total | 2.04 | 0.54 | 2.14 | 2.39 | 2.34 | 1.28 | 1.94 | 1.27 |

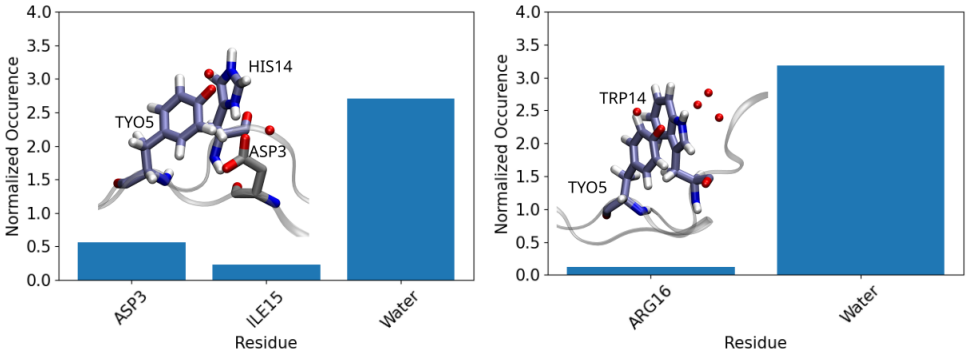


**(a)** β-hairpin peptide H14




**(b)** β-hairpin peptide W14

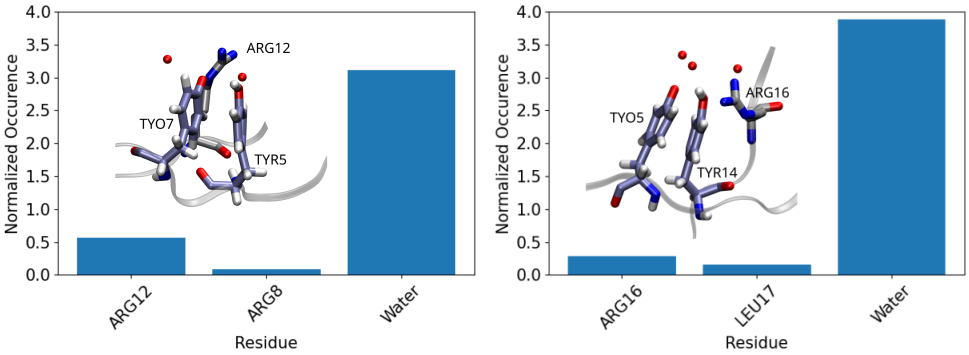


**(c)** β-hairpin peptide Y7




**(d)** β-hairpin peptide Y14s

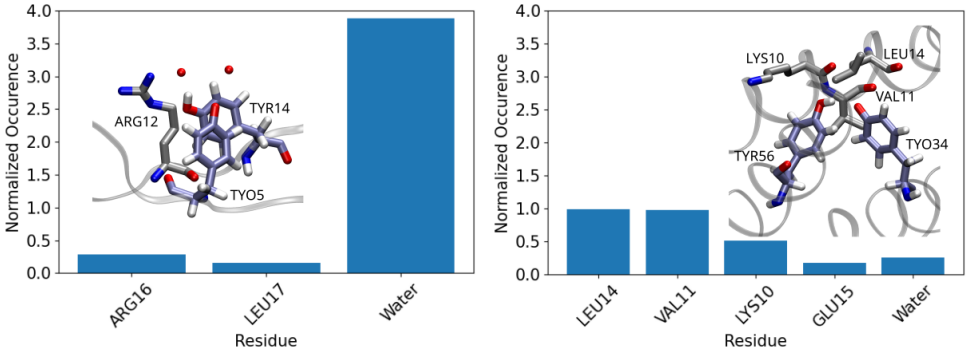


**(e)** β-hairpin peptide Y14f




**(f)** α-helical protein Y56

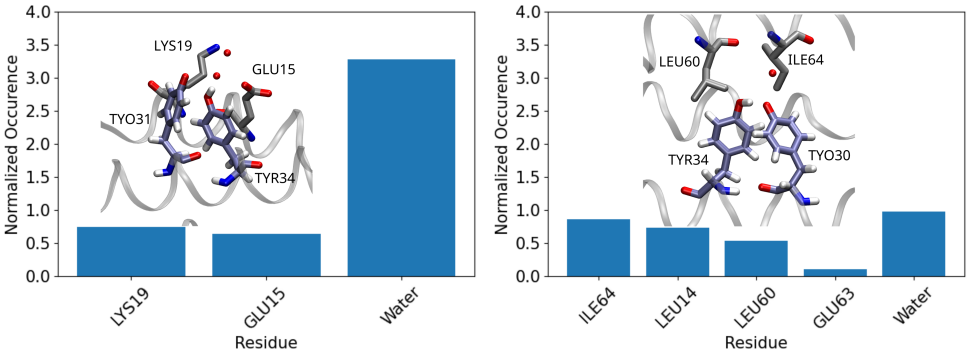


**(g)** α-helical protein Y31




**(h)** α-helical protein Y30

Figure D.2 Bar plots with normalized occurrence of amino acids and water in 3 Å distance of the atoms involved in PCET mechanism for all systems. Only residues with an occurrence $\geq$ 0.05 are displayed.

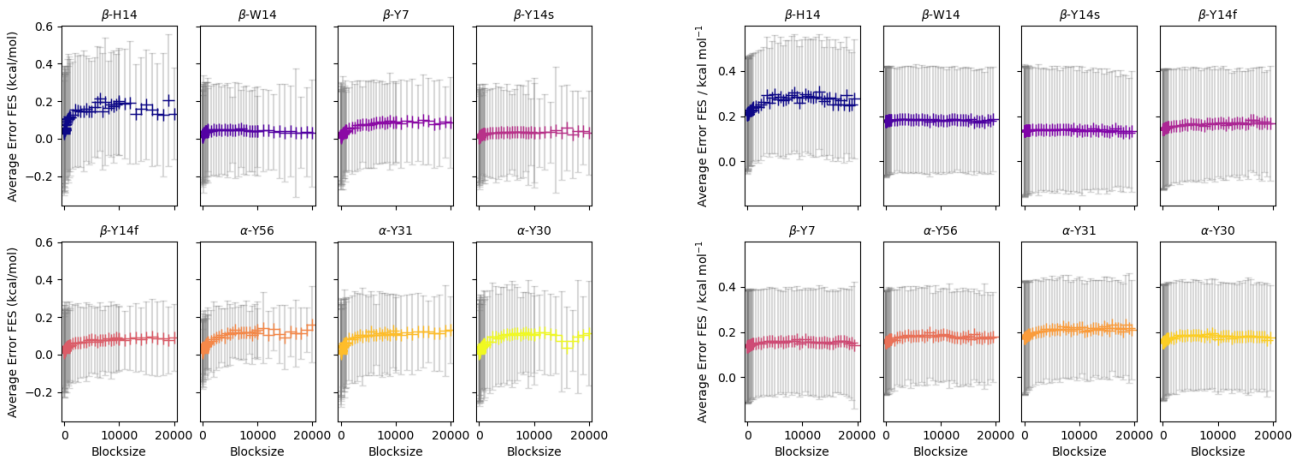


**(a)** 1D **(b)** 2D

Figure E.1 Average free energy error converges to a constant value as block size increases. (a) 1D analysis with biased PT CV only. (b) 2D analysis with biased PT CV and reweighted ET CV.

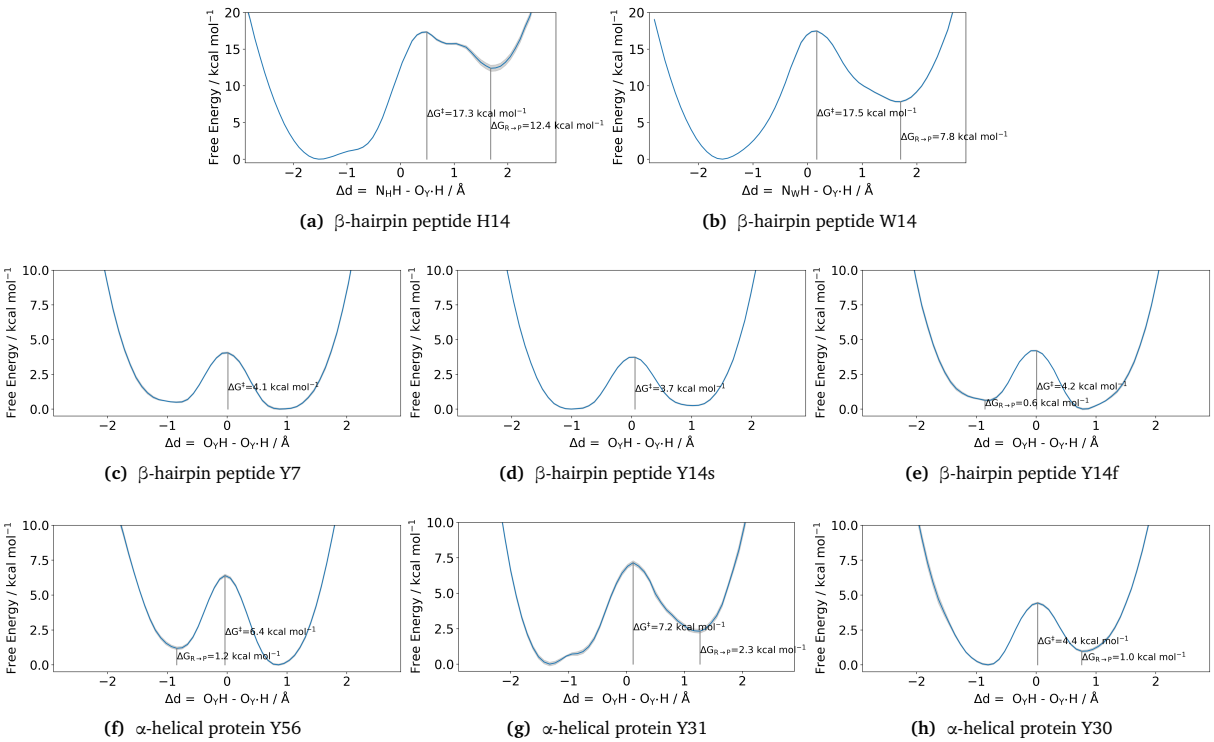


**(a)** β-hairpin peptide H14 **(b)** β-hairpin peptide W14

**(c)** β-hairpin peptide Y7 **(d)** β-hairpin peptide Y14s **(e)** β-hairpin peptide Y14f

**(f)** α-helical protein Y56 **(g)** α-helical protein Y31 **(h)** α-helical protein Y30

Figure E.2 1D free energy surfaces of the proton transfer collective variable. Gray area indicates the error estimate for the free energy.

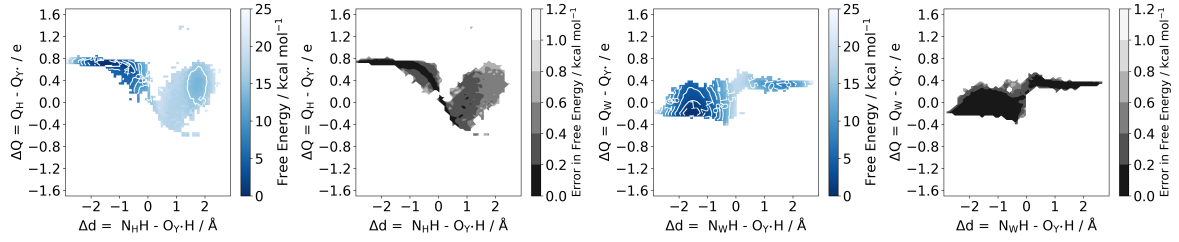


**(a)** β-hairpin peptide H14 **(b)** β-hairpin peptide W14

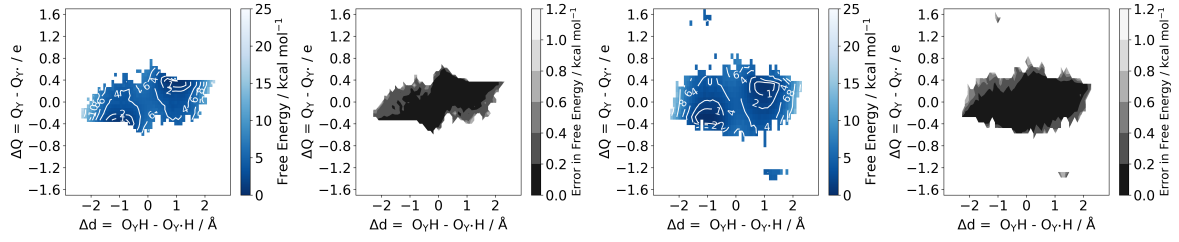


**(c)** β-hairpin peptide Y7 **(d)** β-hairpin peptide Y14s

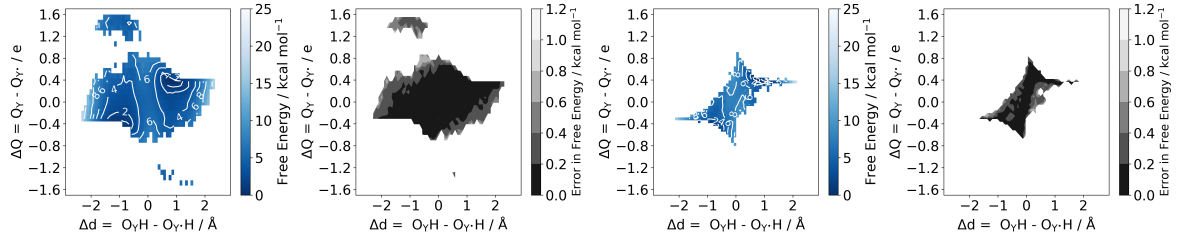


**(e)** β-hairpin peptide Y14f **(f)** α-helical protein Y56

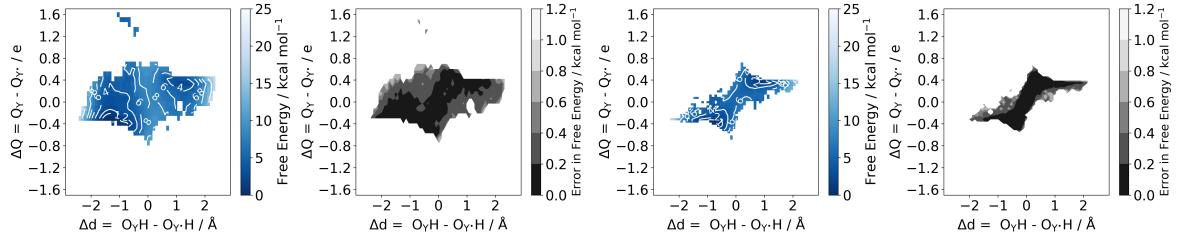


**(g)** α-helical protein Y31 **(h)** α-helical protein Y30

Figure E.3 Free energy surfaces of PCET in all tested systems using DFTB3/MM 1D metadynamic simulations with a bias on the PT reaction coordinate. ET reaction coordinate was corrected at LC-DFTB2/MM level.

### E.2 2D reweighted FES with DFTB3 charges

For comparison purpose the FES of the QM/MM well-tempered metadynamics simulations are shown (Figure E.4) for all biomimetic peptides after applying the reweighting procedure but using DFTB3 for the electron transfer reaction coordinate. The overdelocalization of the excess charge complicates the interpretation of the reaction mechanism, since the electron transfer barrier is absent in most of the systems.

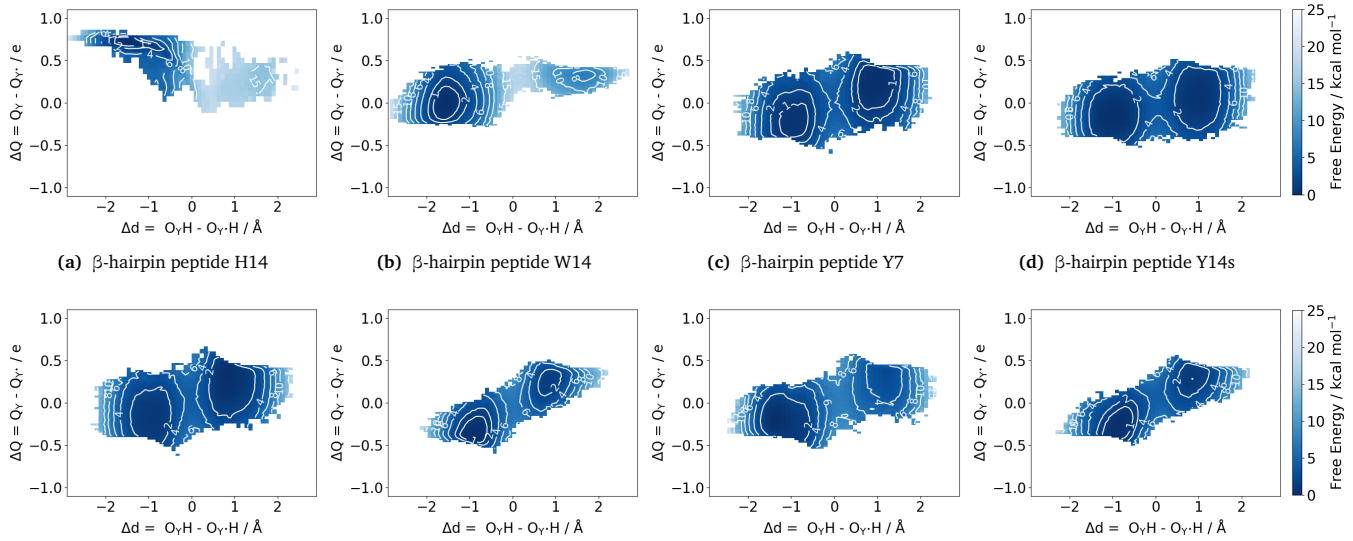


**(a)** β-hairpin peptide H14 **(b)** β-hairpin peptide W14 **(c)** β-hairpin peptide Y7 **(d)** β-hairpin peptide Y14s

**(e)** β-hairpin peptide Y14f **(f)** α-helical protein Y56 **(g)** α-helical protein Y31 **(h)** α-helical protein Y30

Figure E.4 The free energy surfaces show that PCET occurs in all tested systems along the 1D metadynamics simulations, in which the proton transfer reaction coordinate was biased. An electron transfer barrier is observed in α-helical protein Y56 and Y30.

## F OPC water

Simulations using the OPC water model – a 4-point water model recommended for use with the ff19SB forcefield – were carried out for two systems, Y7 and Y31. As shown in Fig. F.1 and F.2, the results closely resemble those obtained with the SPC water model. In β-Y7, the number of water molecules in direct proximity to the tyrosine residues involved in the PCET mechanism increases slightly from 3 to 4 (see Fig. F.1), which also raises the number of hydrogen bonds formed with water from approximately 1.5 to 2. In α-Y31, the number of hydrogen bonds to water remains unchanged at around 1.6, but a slight increase is observed in hydrogen bonding between the tyrosine residues. This change may contribute to the small reduction in the free energy barrier. Notably, π-stacking interactions remain consistent with those observed using SPC water (see Table F.1).

Table F.1 Average number of hydrogen bonds of atoms involved in the PCET reaction either to water molecules (solvent), to other amino acids residues (protein), or between the tyrosine residues for simulations with opc water. π-stacked interactions between aromatic residues involved in the PCET (relative occurrence in % of the trajectory time).

| | β-Y7-opc | α-Y31-opc |
|---|---|---|
| Solvent | 2.07 | 1.62 |
| Protein | 0.00 | 0.06 |
| Tyr˙-Tyr | 0.41 | 0.57 |
| total | 2.49 | 2.25 |
| | | |
| π-stacked | 11.08 | 6.97 |

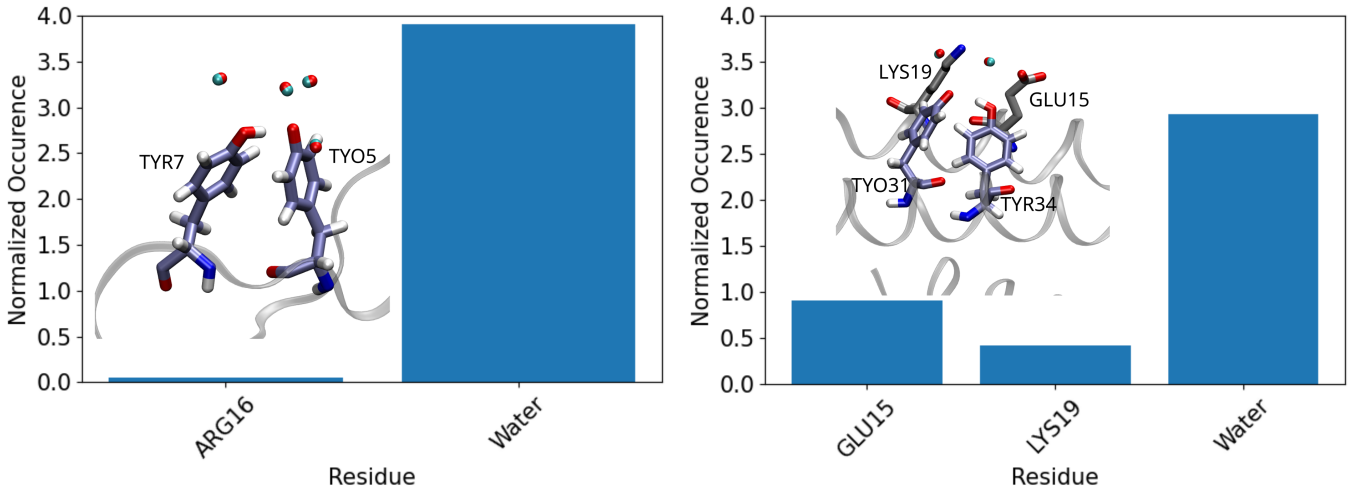


**(a)** Y7 **(b)** Y30

Figure F.1 Bar plots with normalized occurrence of amino acids and water in 3 Å distance of the atoms involved in PCET mechanism for systems simulated with OPC water instead of SPC.

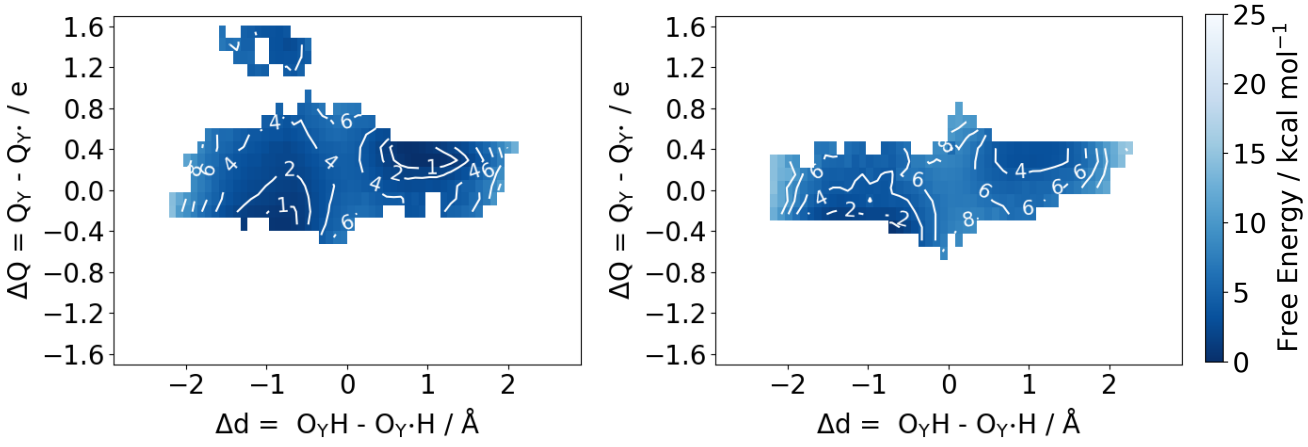


**(a)** Y7 **(b)** Y31

Figure F.2 Free energy surfaces of PCET in systems Y7 and Y31 simulated with OPC water instead of SPC using DFTB3/MM 1D metadynamics simulations with a bias on the PT reaction coordinate.

## References


[1] C. V. Pagba, T. G. McCaslin, S.-H. Chi, J. W. Perry and B. A. Barry, *The Journal of Physical Chemistry B*, 2016, **120**, 1259–1272.

[2] C. V. Pagba, T. G. McCaslin, G. Veglia, F. Porcelli, J. Yohannan, Z. Guo, M. McDaniel and B. A. Barry, *Nature Communications*, 2015, **6**, 10010.

[3] T. G. McCaslin, C. V. Pagba, S.-H. Chi, H. J. Hwang, J. C. Gumbart, J. W. Perry, C. Olivieri, F. Porcelli, G. Veglia, Z. Guo, M. McDaniel and B. A. Barry, *The Journal of Physical Chemistry B*, 2019, **123**, 2780–2791.

[4] U. Uhlin and H. Eklund, *Nature*, 1994, **370**, 533–539.

[5] I. Pujols-Ayala and B. A. Barry, *Biochimica et Biophysica Acta (BBA) - Bioenergetics*, 2004, **1655**, 205–216.

[6] H. B. Gray and J. R. Winkler, *Proceedings of the National Academy of Sciences*, 2015, **112**, 10920–10925.

[7] F. Lacombat, A. Espagne, N. Dozova, P. Plaza, P. Müller, K. Brettel, S. Franz-Badur and L.-O. Essen, *Journal of the American Chemical Society*, 2019, **141**, 13394–13409.

[8] P. Müller, E. Ignatz, S. Kiontke, K. Brettel and L.-O. Essen, *Chemical Science*, 2018, **9**, 1200–1212.

[9] C. R. Reinhardt, P. Li, G. Kang, J. Stubbe, C. L. Drennan and S. Hammes-Schiffer, *Journal of the American Chemical Society*, 2020, **142**, 13768–13778.

[10] C. Tommos, J. J. Skalicky, D. L. Pilloud, A. J. Wand and P. L. Dutton, *Biochemistry*, 1999, **38**, 9495–9507.

[11] B. W. Berry, M. C. Martínez-Rivera and C. Tommos, *Proceedings of the National Academy of Sciences*, 2012, **109**, 9739–9743.

[12] S. D. Glover, C. Jorge, L. Liang, K. G. Valentine, L. Hammarström and C. Tommos, *Journal of the American Chemical Society*, 2014, **136**, 14039–14051.

[13] W. Humphrey, A. Dalke and K. Schulten, *Journal of Molecular Graphics*, 1996, **14**, 33–38.

[14] J. Stone, *MSc thesis*, Computer Science Department, University of Missouri-Rolla, 1998.

[15] D. R. Roe and T. E. Cheatham, *Journal of Chemical Theory and Computation*, 2013, **9**, 3084–3095.

[16] Williams and Kelley, *Gnuplot 4.5: an interactive plotting program*, 2011, `http://gnuplot.info`.

[17] G. Van Rossum and F. L. Drake, *Python 3 Reference Manual*, CreateSpace, Scotts Valley, CA, 2009.

[18] J. D. Hunter, *Computing in Science & Engineering*, 2007, **9**, 90–95.

[19] C. R. Harris, K. J. Millman, S. J. van der Walt, R. Gommers, P. Virtanen, D. Cournapeau, E. Wieser, J. Taylor, S. Berg, N. J. Smith, R. Kern, M. Picus, S. Hoyer, M. H. van Kerkwijk, M. Brett, A. Haldane, J. Fernández del Río, M. Wiebe, P. Peterson, P. Gérard-Marchant, K. Sheppard, T. Reddy, W. Weckesser, H. Abbasi, C. Gohlke and T. E. Oliphant, *Nature*, 2020, **585**, 357–362.

[20] W. McKinney and others, Proceedings of the 9th Python in Science Conference, 2010, pp. 51–56.

[21] M. L. Waskom, *Journal of Open Source Software*, 2021, **6**, 3021.

[22] H. Hwang, T. G. McCaslin, A. Hazel, C. V. Pagba, C. M. Nevin, A. Pavlova, B. A. Barry and J. C. Gumbart, *The Journal of Physical Chemistry B*, 2017, **121**, 3536–3545.

[23] S. Salentin, S. Schreiber, V. J. Haupt, M. F. Adasme and M. Schroeder, *Nucleic Acids Research*, 2015, **43**, W443–W447.